RESEARCH ON THE POLARIZATION IN POROUS OXYGEN ELECTRODES

Contract No. NASW - 1536

Fourth Quarterly Report

Period Covered: January 1, 1968 - March 31, 1968

Issued April 19, 1968

Prepared for

National Aeronautics and Space Administration

Washington D.C.

Written by: Ingemar Lindholm

Ingemar Lindholm
Chemistry Laboratory

Ronny Eriksson
Chemistry Laboratory

Otto von Krusenstierna
Manager Chemistry Laboratory

Approved by: Arne Stomberg
Deputy Director
Central Laboratories

Otto von Krusenstierna
Manager Chemistry Laboratory

ALLMÄNNA SVENSKA ELEKTRISKA AKTIEBOLAGET
Chemistry Laboratory, Fuel Cell Research
Västerås, Sweden

GENERAL SUMMARY

1.1 Program summary

This is the Fourth Quarterly Report (Final Report) of a research program conducted by ASEA under contract with the National Aeronautics and Space Administration, Washington D.C. The objective of this program is an experimental investigation of mass transport polarization and activation polarization in porous oxygen electrodes. Four Quarterly Reports have been issued. The Research summary refers to the total program while the rest of this report refers to work performed during the last quarter.

1.2 Research summary

The research has been directed towards an understanding of the complex processes occuring in porous oxygen cathodes. Such an understanding can result in the identification of rate-limiting processes and ultimately to a rational evolution of electrode structures.

The sequence of steps occuring in a hydrophilic porous oxygen electrode comprise:

a) mass transport of oxygen in gaseous phase

b) mass transport of oxygen molecules through a liquid film

c) mass transport of water to the reaction zone

d) electrosorption of oxygen and electrochemical reaction on the catalyst surface, most likely either as a 2 electron process followed by peroxide decomposition or as a 4 electron process

e) mass transport of OH^--ions from the reaction zone

The experimental results show, that the polarization curves can be divided into three regions with different rate-limiting steps.

The first region occurs at low polarization where the surface reaction is rate-limiting. This region is characterized by a high activation energy, experimentally determined to around 8 kcal/mole, and a deep effective reaction zone, more than 1600 microns. Silver gives a lower polarization than palladium and platinum, presumably due to a difference in electrosorption or faster decomposition of hydrogen peroxide. The polarization vs reversible oxygen electrode in same solution is lower in strong KOH than in weak KOH solutions.

The second region occurs at medium polarization. A combination of mass transport of oxygen by diffusion through liquid films and mass transport of OH^- along the liquid films is rate - - limiting in this region. The polarization is approximatively the same for Ag, Pd and Pt electrocatalysts. The activation energy is lower, around 5 kcal/mole, and the effective reaction zone is thin, around 400 microns. The inverse slope of the

polarization curve at medium polarization $\frac{di}{d\eta}$ is proportional to a mass transport function $\sqrt{S\ D\ \alpha}$ when the oxygen solubility S, oxygen diffusivity D and electrolyte conductivity α, are varied by changing KOH-concentration or temperature.

The exchange current densities for Pd and Pt calculated from our porous electrodes using BET catalyst surface are in agreement with literature values from plane electrodes. The shape of our experimental polarization curves for the first and second region are similar to calculated curves for the thin-film theory when all forms of polarization including the surface reaction with an experimentally determined exchange current density are taken into account.

The third region occurs at very high current densities. The polarization is similar for differing KOH-concentrations, and the current density can be higher than the calculated limiting current density for oxygen diffusivity through the liquid film, even if the rise in electrode temperature is taken into account. Oxygen transport through the liquid film is speeded up by convection in this high-current region.

Experiments with the mixed-gas technique show, that the mass transport of oxygen in gaseous phase increases in importance with increasing current densities. The polarization is lower for an O_2/He-mixture than for a O_2/Ar-mixture of the same composition, showing the influence of the difference in diffusivity for the binary gas mixtures. The mathematical treatment on the "Thin-Film Theory" made by Srinivasan and Hurwitz has been extended to include mass transport in mixed gases. The equations can be used to optimize pore diameter or film thickness for different gas mixtures.

TABLE OF CONTENTS

ABSTRACT

The objective of this investigation is to study mass transport in gas phase and polarization due to it in porous oxygen electrodes. The mixed gas-technique for determination of diffusion effects has been applied. Two inert gases with different binary oxygen/gas diffusivity, argon and helium, have been used.

The polarization has been measured as a function of current density, with varying oxygen conversion and varying oxygen content. The experiments were performed in 4 M KOH at 50°C. The "Thin-Film Model" of Srinivasan and Hurwitz has been extended to include polarization due to mass transport in gas phase for mixed gases.

The current density and current distribution as well as concentration of oxygen at different distances were calculated on a GE 625 computer for different polarization of the oxygen electrode using the modified thin film model.

All polarization data refer to the reversible oxygen electrode in the same solution.

Polarization curves with pure oxygen have been measured up to 1500 mA/cm^2. These data are compared with the calculated limiting current for diffusion of oxygen through a thin liquid film.

LIST OF FIGURES

LIST OF TABLES

2
INTRODUCTION

A large number of investigations have been carried out on the reaction mechanism in the oxygen electrode for various electrocatalysts in acid and in alkaline solution (1-7). However the mass transport in gas phase is in most cases neglected.

Mass transport in oxygen electrodes is often the primary cause of the polarization. This inhibition of reaction may be due to: diffusion of oxygen molecules in the gas phase, diffusion of oxygen in the liquid phase, diffusion or migration of hydroxyl ions in the liquid phase and diffusion of reactant product in liquid or gas phase.

The thin film model derived takes in account diffusion of oxygen in gas phase, diffusion of oxygen in liquid phase, diffusion or migration of hydroxyl ions along the liquid film and activation polarization.

The parameters used in the modified thin film model has been determined in earlier reports and will be used for the calculations.

The mass transport in gas phase is based on the assumption that no convection takes place. At high current density at the same time as the flow is high this assumption is presumably not valid. However the values can be corrected by replacing the diffusivity constant with the "eddy diffusivity". This correction has not been done in this report, since these constants are not known.

The error introduced by the numerical solution is 10 mV. This error can be reduced by an increase in computer run time.

3.1 Physical properties

Electrodes with an active layer of 5 wt% silver were prepared and tested. The thickness of the active layer was 1600 microns. The total thickness including a fine active layer was about 1800 microns.

The BET surface area of the active layer of silver is about 200 cm^2/cm^2 geometric area. The film surface area at a differential pressure of 0.8 atm is 285 cm^2/cm^2 geometric area. The porosity of the active layer is 43.6 %.

Other measured parameters are solubility of oxygen 2.5 10^{-7} mol/cm^3, specific conductance 0.75 ohm^{-1} cm^{-1}, diffusivity of oxygen in 4 M KOH 1.9 10^{-5}.

The electrode temperature was maintained at 50°C.

Diffusivity of oxygen in argon and in helium was calculated using the Chapman-Enskog formula.

The film thickness was measured by means of a gas porosimeter, and the value $1 \cdot 10^{-4}$ cm was obtained.

The pore radius was estimated to $2 \cdot 46\ 10^{-4}$ cm by means of microscopephotos, surface tension and dilatometer measurements.

The exchange current density was estimated from measurements at low current densities to approximately 10^{-7} A/cm^2.

3.2 Arrangement for testing of electrodes

The gas pressure was measured with a precision manometer and at the same time recorded with a pressure gauge in order to see any fluctiation of the pressure during the run.

Preheating was arranged by letting the gas mixture pass a coil of aluminium immersed in the bath before the entrance in the electrode holder. To keep a constant conversion a high vacuum valve was used for flow regulation of the gas mixture. Before the entrance to the gas chromatograph the gas mixture was dried with magnesium perchlorate. The flow was measured at atmospheric pressure with a soap bubble tube. The conversion was recorded with a Perkin-Elmer gaschromatograph F6/3T. The following conditions were used:

Column: Molecular sieve 2 micron

Column temp.: 50°C

Reference gas: Argon or helium as the case may be

Reference gas flow: 50 ml/min.

Bridge voltage: 5.25 Volt

Gas pressure: 3.5 bar

3.3
Electrochemical Measurements on Electrodes

Investigation of polarization curves of varying oxygen content in argon as well as in helium were made at 50°C in 4 M KOH at optimum differential pressure. The measurements were done with porous electrodes of nickel with silver as electrocatalyst in a coarse, porous layer and nickel in a fine, porous layer facing the electrolyte side.

The electrocatalytic activity was measured in half-cells with Ø 35 mm porous discs as oxygen electrodes in a holder.

I-v curves are measured stepwise with an interval of 3 minutes. The mV-meter has an internal resistance of $10^{14}\ \Omega$. The duration of the measurements was one day. Each solution was titrated to ± 0.05 mol/l. The half cell used for current potential measurements is shown in fig. 1. The cell is heated by a water bath. Potential were measured with a mV-meter (Radiometer PHM 22) by means of a Luggin capillary with tip placed in the centre of the electrodes 1 mm from the surface.

Current is supplied by an ASEA-galvanostat, fig. 1. The reference electrode is a hydrogen electrode with nickel-boride electrocatalyst in 7 M KOH at 50°C with a pressure of 2.6 bar. The RI-drop, between the tip of the reference capillary and the electrode surface, is measured by rapid breaking of current with a Hg-relay, trigged to a storage oscilloscope (Tektronix 564). This purely ohmic voltage drop decays faster than 1 microsecond and can easily be distinguished from other slower decay. All measured values have been corrected this way. All instrument used has been checked by comparison with references. Optimum differential pressure was obtained by increasing the pressure at - 350 mV polarization until the current reaches a maximum.

4
EXPERIMENTAL RESULTS

4.1
Electrochemical tests with the mixed-gas technique

Fig. 3 shows experimental polarization curves for oxygen - - argon mixtures at a low conversion of oxygen. It is apparent that the polarization is much larger at higher current densities with a low oxygen content in the gas mixture.

Fig. 4 shows experimental polarization curves for oxygen - - helium mixtures at a low conversion of oxygen. The shape of the curves are similar to the oxygen - argon curves.

Fig. 5 shows a comparison of the polarization for different oxygen - argon and oxygen - helium mixtures at a relatively high current density, 300 mA/cm^2. Oxygen - helium mixtures have less polarization than oxygen - argon mixtures especially at low oxygen contents. As the oxygen diffusivity is 4 - 5 times lower in the argon mixtures it can be concluded that the mass transport in the gas phase in the pores has a rate limiting influence.

Fig. 6 shows polarization curves for 20 % oxygen and 80 % argon at varying conversion of oxygen. High conversion of oxygen when the gas mixture passes the electrode gives a higher polarization due to the lower content of oxygen in gas phase near the electrode. There is also a limiting current density depending on mass transport in gaseous phase.

4.2 Comparison of experimental data with numerical calculations

Fig. 7 and 8 shows a comparison between experimental polarization curves and calculated polarization curves for gas mixtures. The calculations are based on the "Thin film model" and include mass transport in gaseous phase. The technique used is discussed in the Appendix. The calculated data have higher polarization than the experimental, and a limiting current density at a lower value than the experimental curves.

It is of course very difficult to carry out numerical calculations on the total process in a porous electrode. The exchange current density, i_o, in only an approximation of the rate constant for the surface reaction as the mechanism for this may change with the potential. The pore system in a real electrode contains an uneven film with a very curved surface which is difficult to take into account in the "Thin film theory"; although tortuosity factors were measured in the Third Quarterly Report (ref. 10). The lower polarization in the experimental curves could be caused by convection in gaseous phase, so-called "eddy diffusivity".

Concentration profiles for oxygen concentration, current distribution and surface concentration of oxygen at the bottom of the pore have been calculated for 20 % oxygen - - 80 % helium mixture, and are shown in tables 1-3.

At a low current density there is no significant difference between helium and argon, but helium gives a lower polarization than argon at a certain current density: About 20 mA/cm^2 for 10 % O_2, 60 mA/cm^2 for 20 % O_2 and 150 mA/cm^2 for 40 % O_2.

The theoretical model shows that oxygen in helium has a lower polarization than oxygen in argon due to the difference in diffusion constants in gaseous phase, D_g = 0.56 cm^2/s for oxygen - helium and 0.12 cm^2/s for oxygen - argon.

At lower current densities, the oxygen diffusion in gaseous phase will cause less polarization than the surface reaction. At higher current densities the length of the active reaction zone will depend on the transport properties of the mixed gases.

The mass transport in liquid phase along the film limits the film thickness to relatively thick films. The mass transport in gaseous phase for mixed gases is more when the open volume is larger in the pore system. This means that there exists an optimum pore radius for a given film thickness. This optimum radius gives rapid oxygen transport in gaseous phase as well as ionic transport along the film and mass transport of oxygen molecules through the liquid film.

The numerical solution was obtained using steps of $1/20^{th}$ of pore length. This results in uncertain values at low and high current densities. The error limit for voltage drop introduced in the numerical calculation is less than 10 mV. Further reduction in this error is only a matter of more computer time.

CALCULATED CONCENTRATION PROFILES OF OXYGEN IN A MIXTURE OF 20 % OXYGEN AND 80 % HELIUM

Table 1

$C \cdot 10^9$ mol O_2/cm^3

Z/L \ η	0	.1	.2	.3	.4	.5	.6	.7	.8	.9	1.0
0	93	93	93	93	93	93	93	93	93	93	93
.2	93	92	91	80	30	9.1	7.8	7.6	7.6	7.6	7.6
.4	93	88	65	1.3	0.7	0.6	0.6	0.6	0.6	0.6	0.6
.6	93	38	0.07	0.05	0.0	0.0	0.0	0.0	0.0	0.0	0.0
.8	93	0	0.0	0.01	0.0	0.0	0.0	0.0	0.0	0.0	0.0
1.0	93	0	0.0	0.0	0.0	0.0	0.0	0.0	0.0	0.0	0.0

Parameters are:

$R2 = 2.46 \cdot 10^{-4}$ cm $R1 = 1.46 \cdot 10^{-4}$ cm $L = 0.16$ cm $Af = 285$ cm^2/cm^2

$D_g = 0.56$ cm^2/s $D_i = 1.9 \cdot 10^{-5}$ cm^2/s $Sb_{O_2} = 2.5 \cdot 10^{-7}$ mole/$cm^2 \cdot$ atm

$X_{O_2} = 0.164$ $Po = 1.80$ atm $i_o = 1.5 \cdot 10^{-7}$ A/cm^2

$T = 323^{\circ}K$ $\kappa = 0.75 \Omega^{-1}$ cm^{-1} $m \cdot F = 4 \cdot 96500$ As

Voltage error 20 mV

Steps 20 st

CALCULATED CURRENT DISTRIBUTION IN A MIXTURE OF 20 % OXYGEN AND 80 % HELIUM

Table 2

$I = 10^{7}$ A/pore

Z/L \ η	0	.1	.2	.3	.4	.5	.6	.7	.8	.9	1.0
0	0	0.1	0.5	3.2	18	81	190	250	260	260	260
.2	0	0.1	0.5	3.2	16	21	21	22	22	22	22
.4	0	0.1	0.5	1.8	2	2	2	2	2	2	2
.6	0	0.1	0.1	0.1	0.1	0.1	0.1	0.1	0.1	0.1	0.1
.8	0	0	0	0	0	0	0	0	0	0	0
1.0	0	0	0	0	0	0	0	0	0	0	0
	0	0.8	3.1	15.2	6	61	293	356	366	366	366

Parameters are the same as in table 1

Table 3

CALCULATED SURFACE CONCENTRATION OF OXYGEN AT BOTTOM OF PORE

η	$C(L, r_2)$
0	$9.27 \cdot 10^{-8}$
0.2	$8.8 \cdot 10^{-11}$
0.4	$1.3 \cdot 10^{-12}$
0.6	$3.4 \cdot 10^{-14}$
0.8	$9.4 \cdot 10^{-16}$
1.0	$2.5 \cdot 10^{-17}$

Parameters are the same as in table 1

LIMITING CURRENT DENSITY, PURE OXYGEN

The experimental equipment for electrochemical measurements was the same as in earlier measurements (8, 9, 10) but a thin thermocouple was attached to the gas side of the electrodes. The high current was supplied from a 12 V battery in series with a resistor. Polarization curves were measured at optimum differential pressure for electrodes with 100 and 400 microns active layer containing a silver electrocatalyst. 100 % oxygen was used in these measurements.

Fig. 10 shows a polarization curve for an electrode with 400 microns active layer containing silver electrocatalyst (compared with an electrode without electrocatalyst). The optimum differential pressure oxygen-electrolyte was 1.0 atm. The shape of this curve is the same as measured earlier up to 400 mA/cm^2. There is an increase in polarization up to 900 mA/cm^2 and a slow decrease in polarization at higher current densities. This decrease was unexpected as the earlier tests up to 400 mA/cm^2 did not show a decrease in polarization for 4 M KOH.

The influence of local temperature must be taken into account in reaction kinetic measurements at high current densities. This temperature increases from 50°C up to 69°C at 1500 mA/cm^2 causing an increase in oxygen diffusivity in KOH from $1.9 \cdot 10^{-5}$ cm^2/s to $3.5 \cdot 10^{-5}$ cm^2/s and an increase in electrolyte conductivity from 0.75 $ohm^{-1}\ cm^{-1}$ to 0.96 $ohm^{-1}\ cm^{-1}$. These changes are probably not large enough to cause a decrease in polarization if the total reaction cycle remains unchanged. The interesting decrease in polarization at high current densities stimulated further experiments with a thinner active layer in order to study the mechanism.

The electrode of nickel without electrocatalyst gives a low current density even at high polarization. It is evident that the silver surface is involved in the majority of the reaction.

Fig. 11 shows a comparison of polarization curves for an electrode with only 100 microns active layer thickness in 4 M KOH, 7 M KOH and 10 M KOH electrolyte. The optimum differential pressure oxygen-electrolyte was 1.4 atm at all KOH-concentrations.

These polarization curves can be devided into three regions.

In region 1, low polarization up to about - 350 mV vs a reversible oxygen electrode there is only a small difference between the curves with a higher polarization in weak 4 M KOH electrolyte.

In region II, medium polarization from - 350 mV to about - 600 mV there are approximatively linear polarization curves. The slope is steepest in strong 10 M KOH giving the highest polarization in strong KOH-electrolyte.

Table 4 Comparison between calculated limiting currents for diffusion of oxygen through a liquid film and measured currents.

Active layer thickness microns	KOH-concentration M	P_{O_2} diff. atm	Interface gas-liquid $\frac{cm^2}{cm^2}$ geom.	Interface liq.-solid $\frac{cm^2}{cm^2}$ geom.	Catalyst surface $\frac{cm^2}{cm^2}$ geom.	Vol. % gas in pores	Film thickness microns	Calc. i_l 50°C mA/cm^2	Calc. i_l 70°C mA/cm^2	Measured i mA/cm^2	Measured "real c.d." catalyst area mA/cm^2
400	4	1.0	88	320	60	53	0.93	3500	6400	1500	25
100	4	1.4	35	80	15	71	0.37	4200	7200	1500	100
100	7	1.4	35	80	15	71	0.37	880	1600	1500	100
100	10	1.4	35	80	15	71	0.37	220	410	1200	80

These two regions have been treated in detail in our Quarterly Report No 2. The rate-determining step in region I is the reaction on the surface. The rate-determining step in region II is a combination of mass transport of OH^- by migration and diffusion along the liquid film by a diffusion mechanism. Ordinary fuel cells operate mainly in this region.

In region III, high polarization, more than - 600 mV vs reversible oxygen, there is a difference in the shape of the curves. The curves for 7 M KOH and 10 M KOH gets less steep and the slope of the three curves are almost the same at high current densities. There is a tendency to get almost the same polarization in 4 M KOH and 7 M KOH, in spite of the large difference in oxygen solubility and diffusivity, which are considerably lower in 7 M KOH. The OH^- concentration in the liquid films is increased during the reaction due to formation of OH^--ions. This would cause a further decrease in oxygen solubility and diffusivity at high current densities and a steeper polarization curve at high current densities, while the experimental curves are almost horisontal at high current. This suggests, that a new mechanism for mass transfer is operating.

The limiting current densities for gas diffusion through a liquid film can be calculated from the formula

$$\frac{D_{n_{O_2}}}{dt} = \frac{S \cdot D \cdot A}{W}$$

The film surface A and film thickness W have been determined by gas porosimeter experiments (Quarterly Report 3, ref. 10). Oxygen solubility S and diffusivity D for the bulk solution were used in our calculations (these values are smaller in the film). Limiting current densities were calculated both for bulk solution temperature 50°C and electrode temperature 70°C and are shown in table 4.

It is evident, that the measured current density is much higher than the calculated value for 10 M KOH.

The difference in mechanism is probably that convection occurs in the liquid film causing rapid transport of O_2 molecules through the film. This can either be caused by the large heat evolved in the solid-liquid interphase or by the gradient in liquid tension, the Marangoni effect, as suggested by Will (11) and Ksenshek (12) for model electrodes.

Table 4 also shows that the current density calculated on real electrocatalyst surface area can be very high more than 100 mA/cm2 on silver.

6 CONCLUSIONS

The experimental mass transport test with mixed-gas technique shows that there is a significant difference between oxygen in helium and oxygen in argon, especially for low oxygen contents. This proves that the difference in polarization - - lower in oxygen - helium mixtures with a high oxygen diffusivity - is due to differences in mass transport in the gaseous phase.

It can therefore be concluded that at low oxygen contents, there is a limiting current due to mass transport in the gaseous phase.

For mixed gases and a given film thickness, there is an optimum pore structure where the mass transport in both gaseous phase and liquid phase are rapid. This structure is different from an optimum structure for pure oxygen.

Calculations according to the "Thin film theory" show that the current is evenly distributed along the pore for a low polarization. At a high polarization, most of the current comes from the part near the gas side when the electrode is supplied with an oxygen - inert gas mixture, and the concentration of oxygen is very small in the pores near the electrolyte side. This current distribution profile is very different from operation on pure oxygen at high polarization, where most of the current is generated in the bottom of the coarse layer pores near the fine layer and free electrolyte.

Experiments with pure oxygen indicate that convection in liquid films increases the rate of mass transport of oxygen molecules through these films at high current densities. Current densities of 1500 mA/cm^2 have been reached with a 100 micron thin active layer. These data correspond to a "real current density" of 100 mA/cm^2 on the silver electrocatalyst surface area.

These experiments demonstrate the possibility to get more rapid mass transport of oxygen through the liquid films than calculated from diffusion. An electrode with a modified structure to give less resistance along the liquid films and more electrocatalyst surface area would give less polarization at these high current densities. This is a promising approach to achieve higher energy density fuel cells.

7 RECOMMENDATIONS

In order to arrive at improved oxygen electrode systems further research in the following areas is indicated.

a) Investigation of the reaction kinetics in the high current density region including determination of the electrolyte concentration in the liquid films.

b) Direct measurements of oxygen electrosorption on varying electrocatalysts with varying KOH-concentration and electrode potential.

c) Manufacture electrodes with varying pore structure and electrocatalyst surface area. The film area and film resistance for each structure are measured and compared with the corresponding current density - differential pressure and polarization curves.

8
BIBLIOGRAPHY

1. Hoare, J.P.: J. Electrochem. Soc. 112 (1965), p. 602
2. Hoare, J.P.: J. Electrochem. Soc. 112 (1965), p. 1129
3. Yeager, E., Davies, M.D., Clark, M., Hovorka, F.: J. Electrochem. Soc. 106 (1956), p. 56
4. Vielstich, W.: Z. Physik. Chem. 15 (1958), p. 409
5. Sawyer, D.T., Day, R.J.: Electrochemica Acta 8 (1963), p. 5
6. Bockris, J.O.M., Srinivasan, S.: Journées Internationales d'Etude des piles à Combustibles, Brussels, June 21-24, 196
7. Lingane, R.: J. Electrochem, Soc. 110 (1961), p. 269
8. Lindholm, I., Edwardsson, I.: NASW-1536. First Quarterly Report April 1 - June 30, 1967
9. Lindholm, I., Edwardsson, I.: NASW-1536. Second Quarterly Report July 1 - Sept 30, 1967
10. Lindholm, I., Edwardsson, I.: NASW-1536. Third Quarterly Report Oct 1 - Dec 31, 1967
11. Will, F.G.: Deuxieme Journées Internationales d'Etude des Piles à Combustibles. Bruxelles June 1967.
12. Ksenshek, O.S.: Deuxieme Journées Internationales d'Etude des Piles à Combustibles. Bruxelles June 1967
13. Srinivasan, S, Hurwitz, H D: Electrochimica Acta 12 495 1967

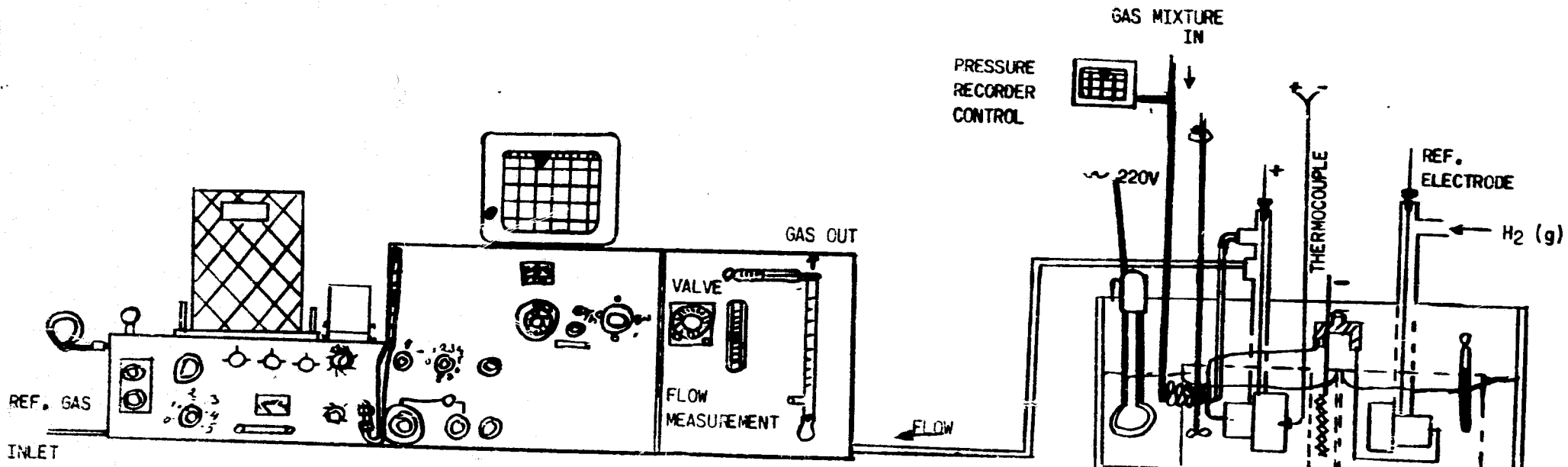

GAS CHROMATOGRAPH
PERKIN-ELMER F6/3T

NICKEL BATH

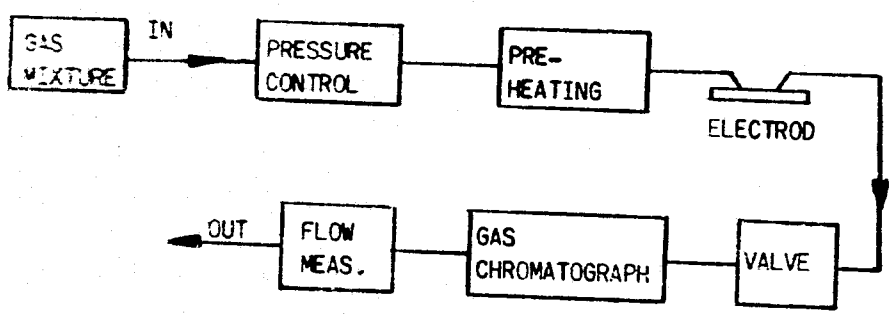

SCHEMATIC GAS FLOW

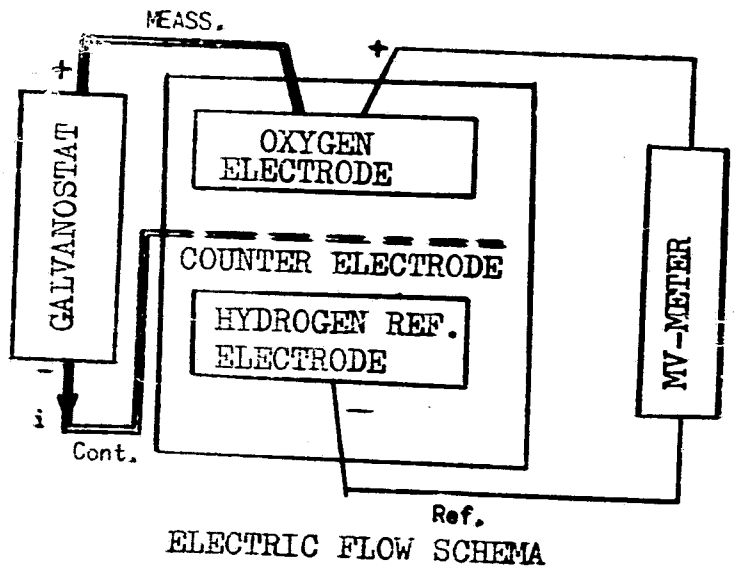

ELECTRIC FLOW SCHEMA

FIG. 1 ARRANGEMENT FOR ELECTRODE TESTING

FIG. 2 ARRANGEMENT FOR CURRENT - VOLTAGE CURVES

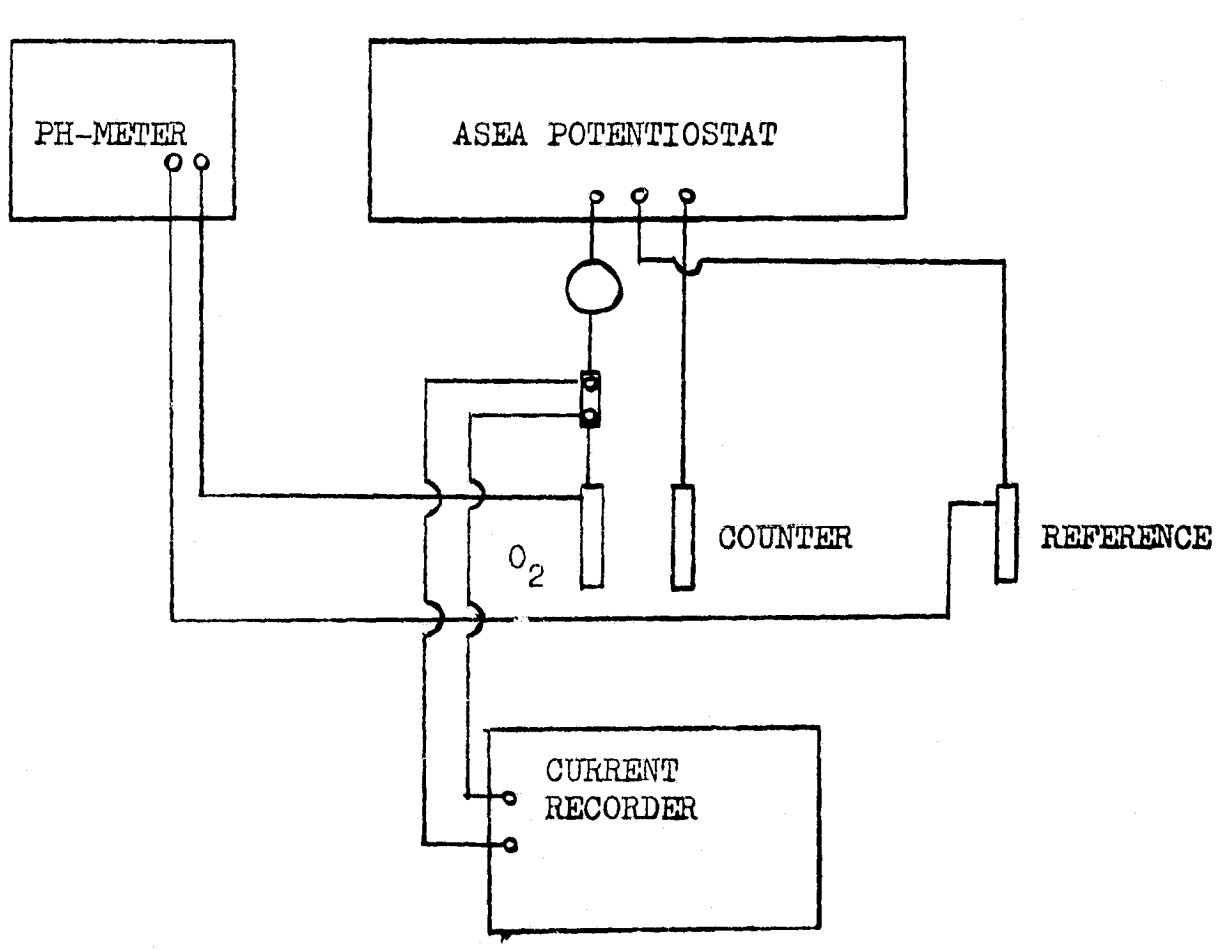

FIG. 3 POLARIZATION CURVES AT OPTIMUM DIFFERENTIAL PRESSURE AT VARYING OXYGEN CONTENT IN ARGON

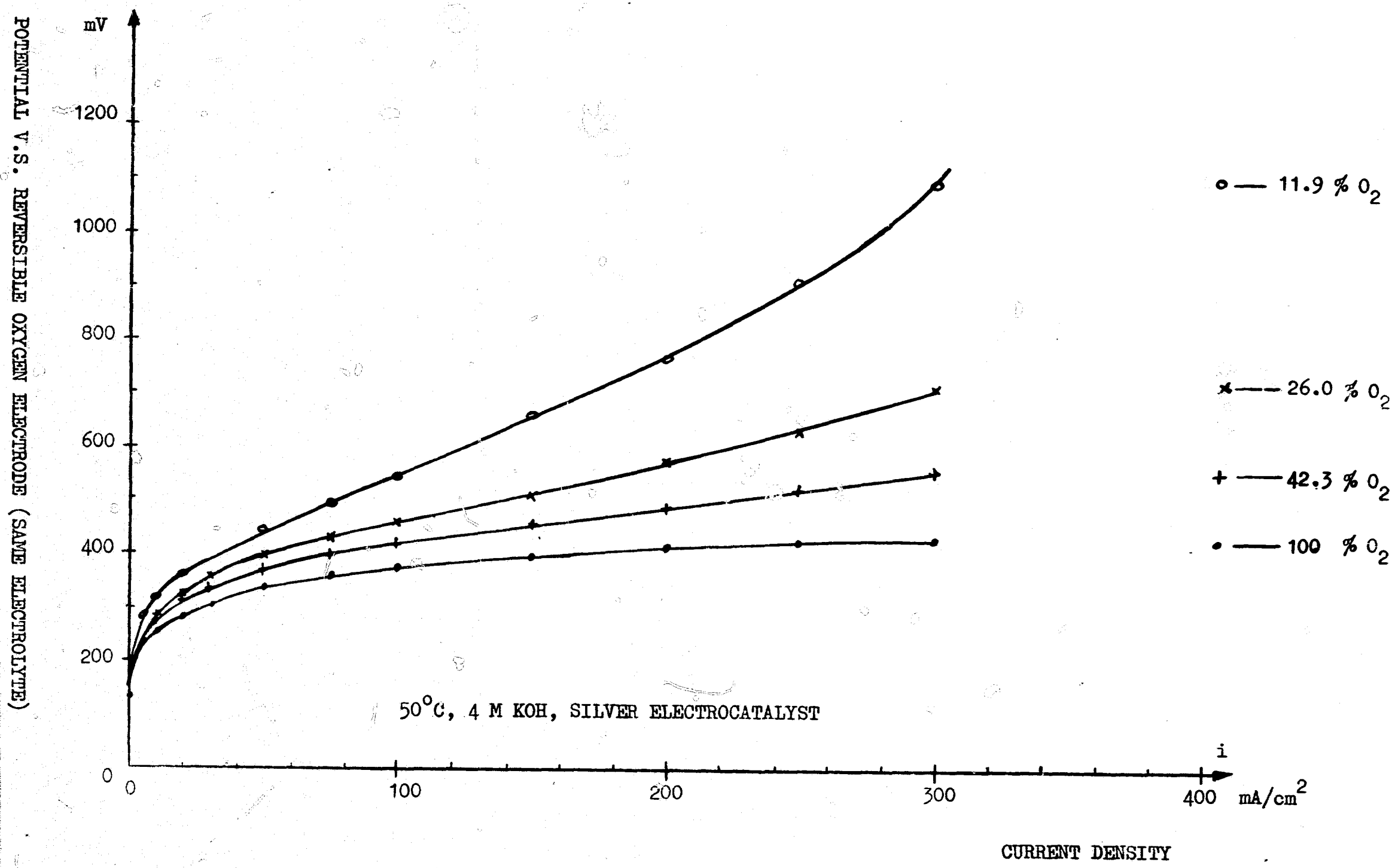

FIG. 4 POLARIZATION CURVES AT OPTIMUM DIFFERENTIAL PRESSURE AT VARYING OXYGEN CONTENT IN HELIUM

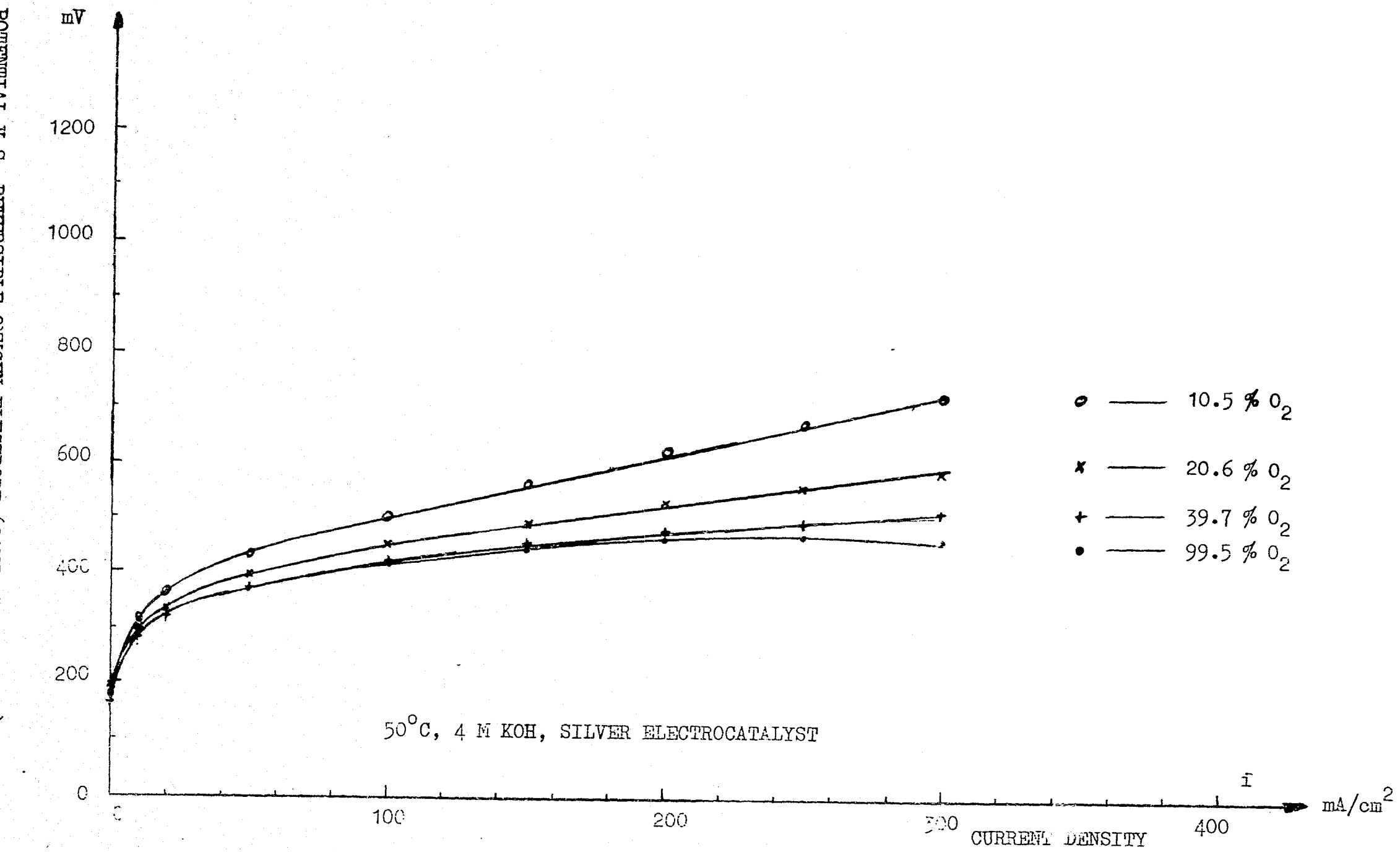

FIG. 5 POLARIZATION AT 300 mA/cm^2

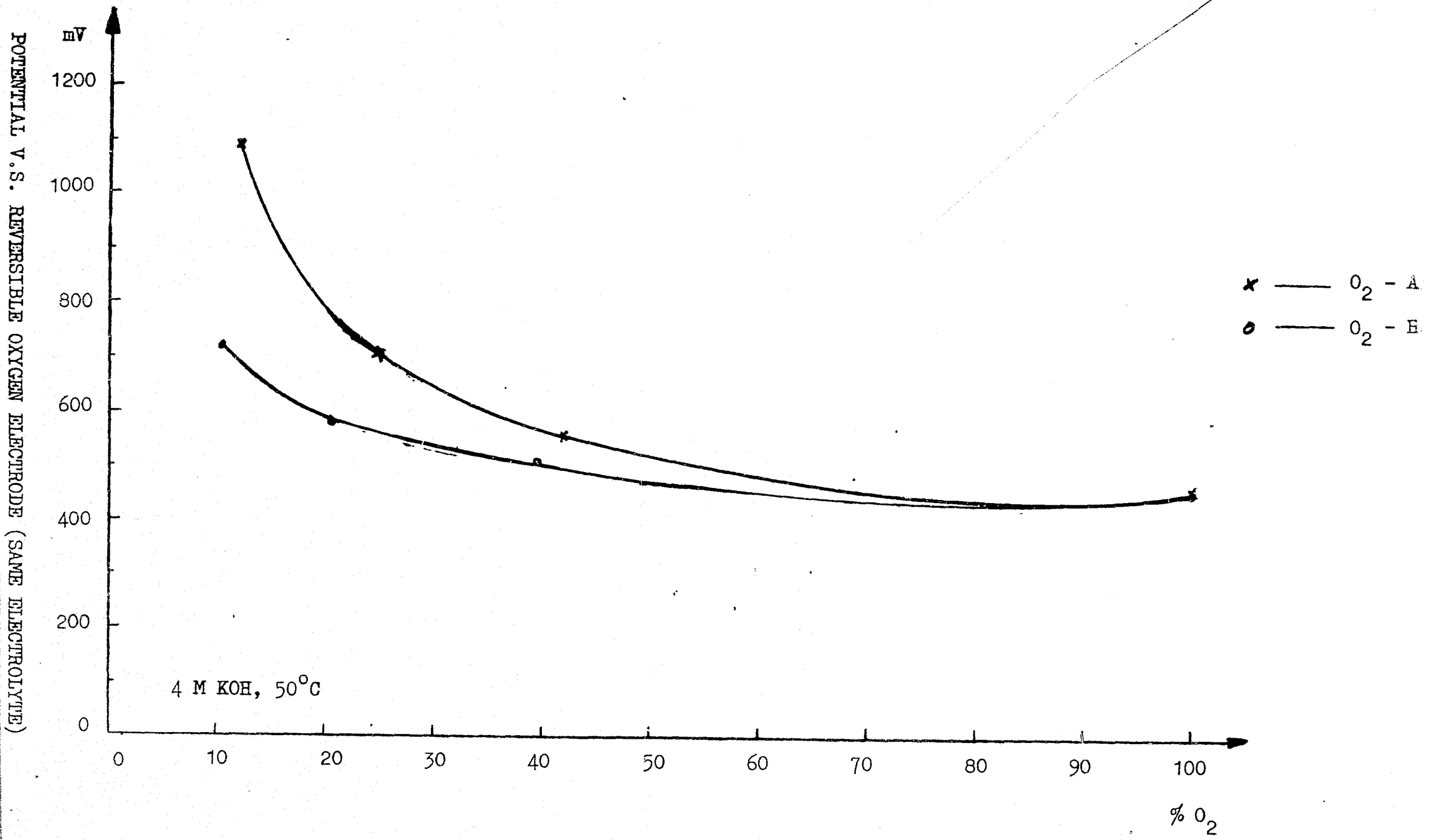

FIG. 6 POLARIZATION CURVES AT OPTIMUM DIFFERENTIAL PRESSURE FOR 20 % OXYGEN IN ARGON AT VARYING CONVERSION OF OXYGEN

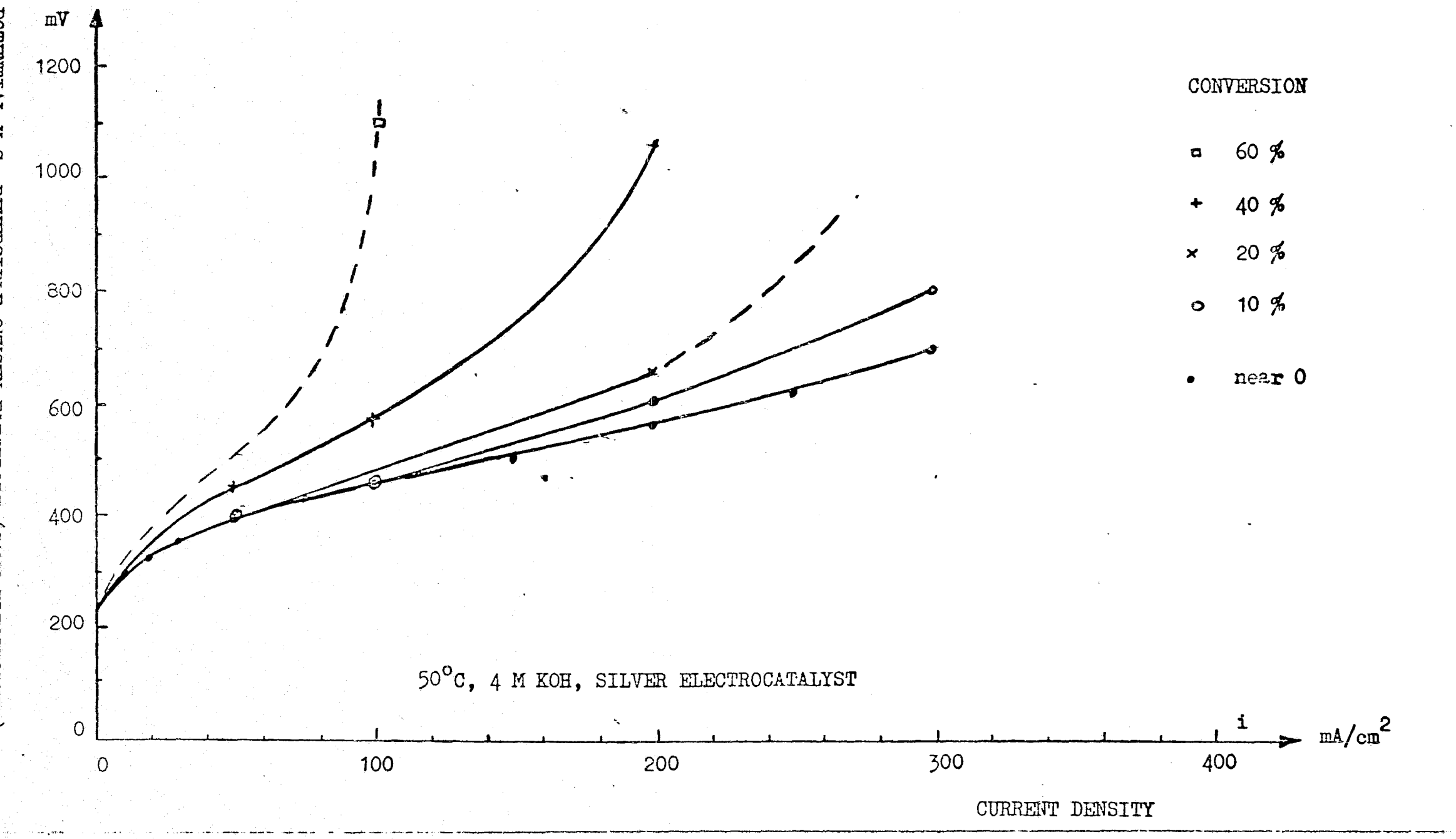

FIG. 7 COMPARISON BETWEEN CALCULATED AND EXPERIMENTAL CURVES FOR OXYGEN IN ARGON

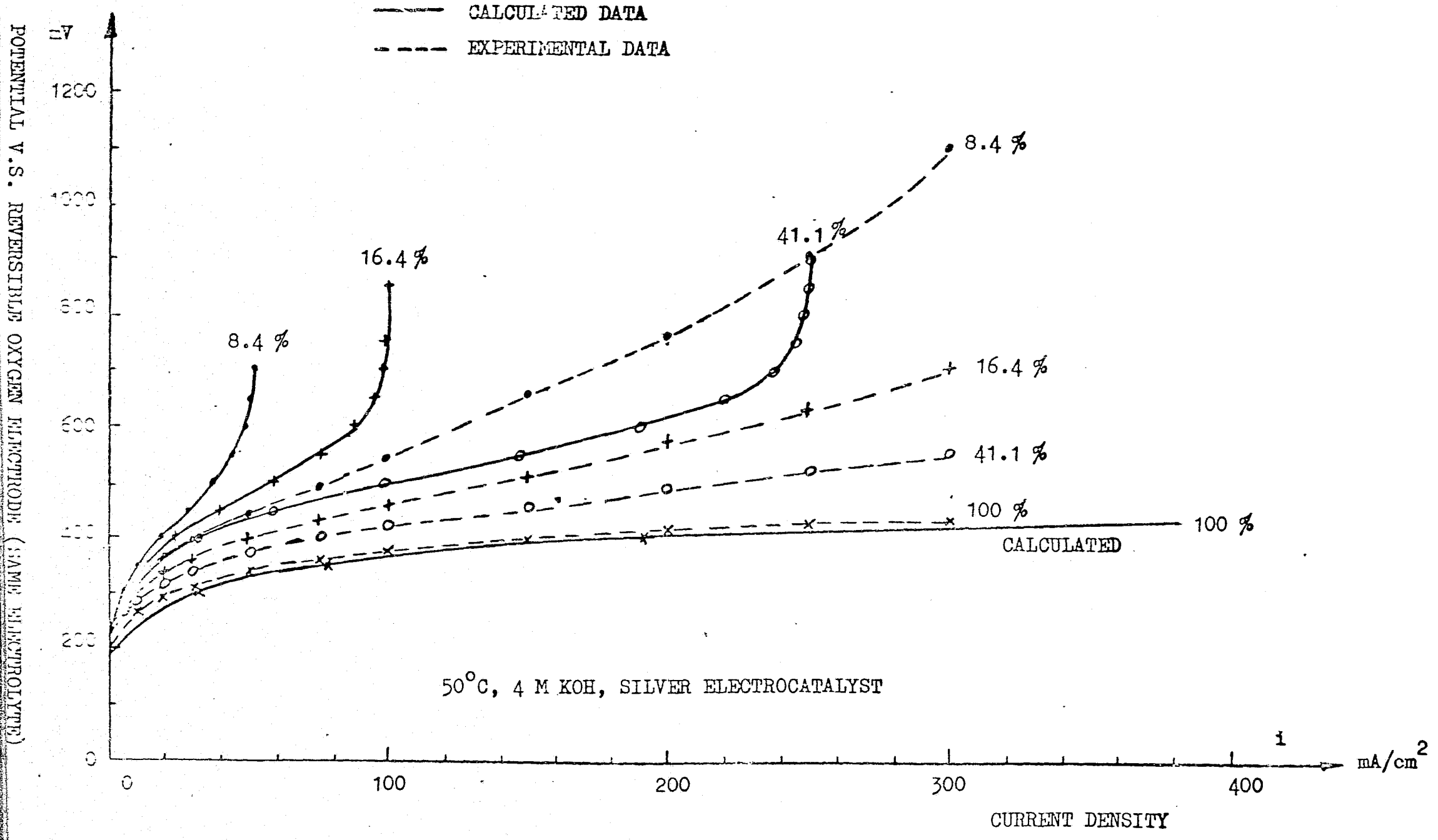

FIG. 8 COMPARISON BETWEEN CALCULATED AND EXPERIMENTAL CURVES FOR OXYGEN IN HELIUM

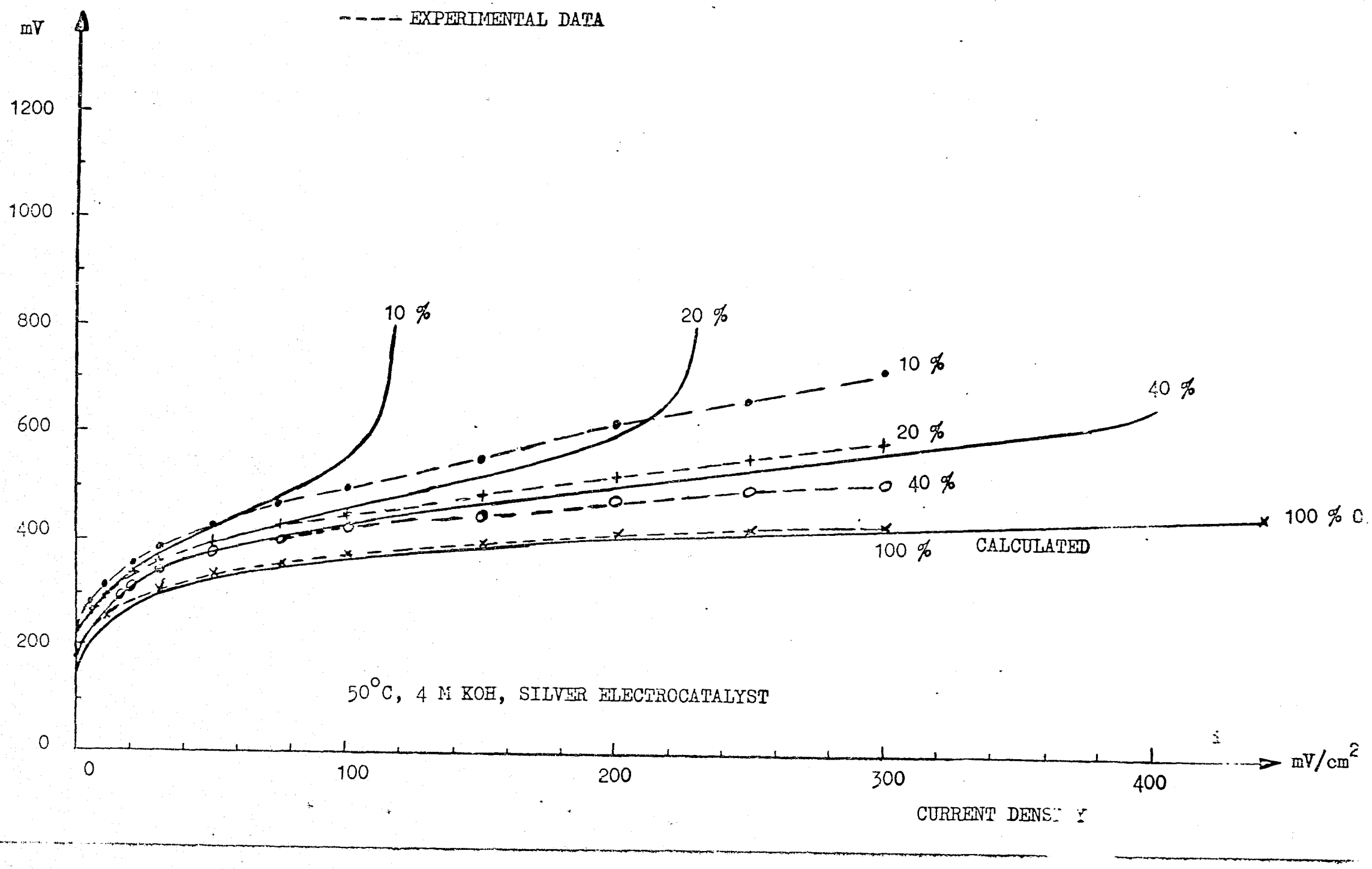

FIG. 9 PORE MODEL

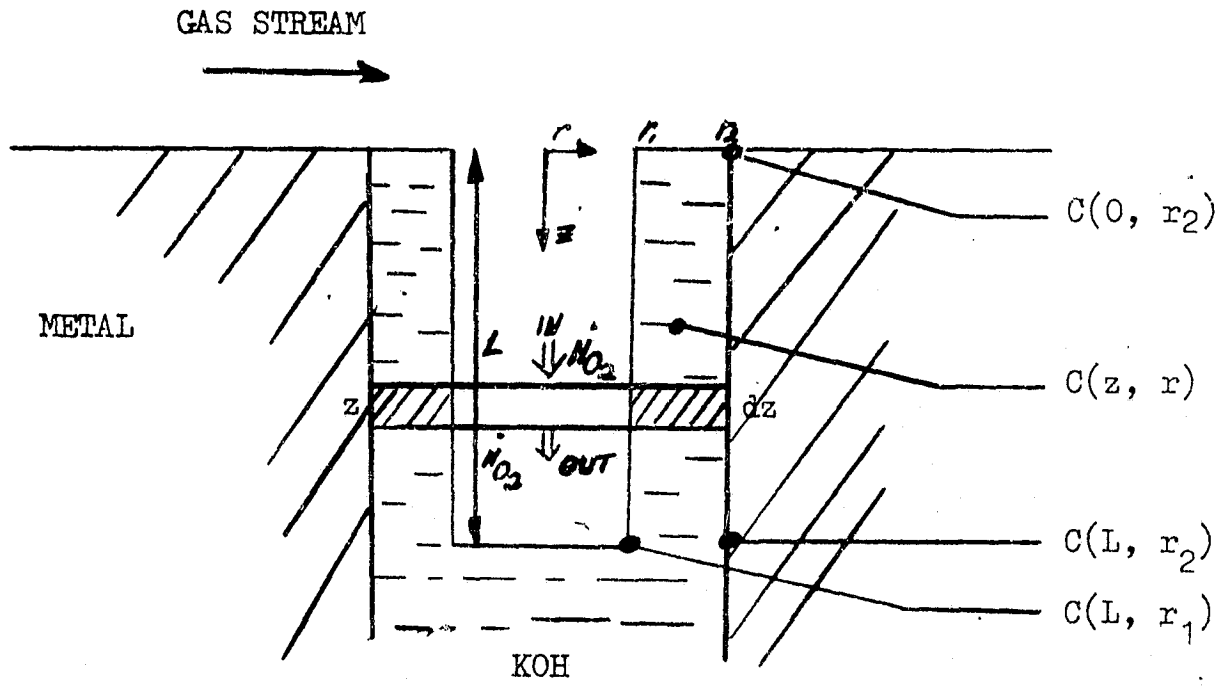

FIG. 10 POLARIZATION CURVES AT OPTIMUM DIFFERENTIAL PRESSURE 1.0 ATM

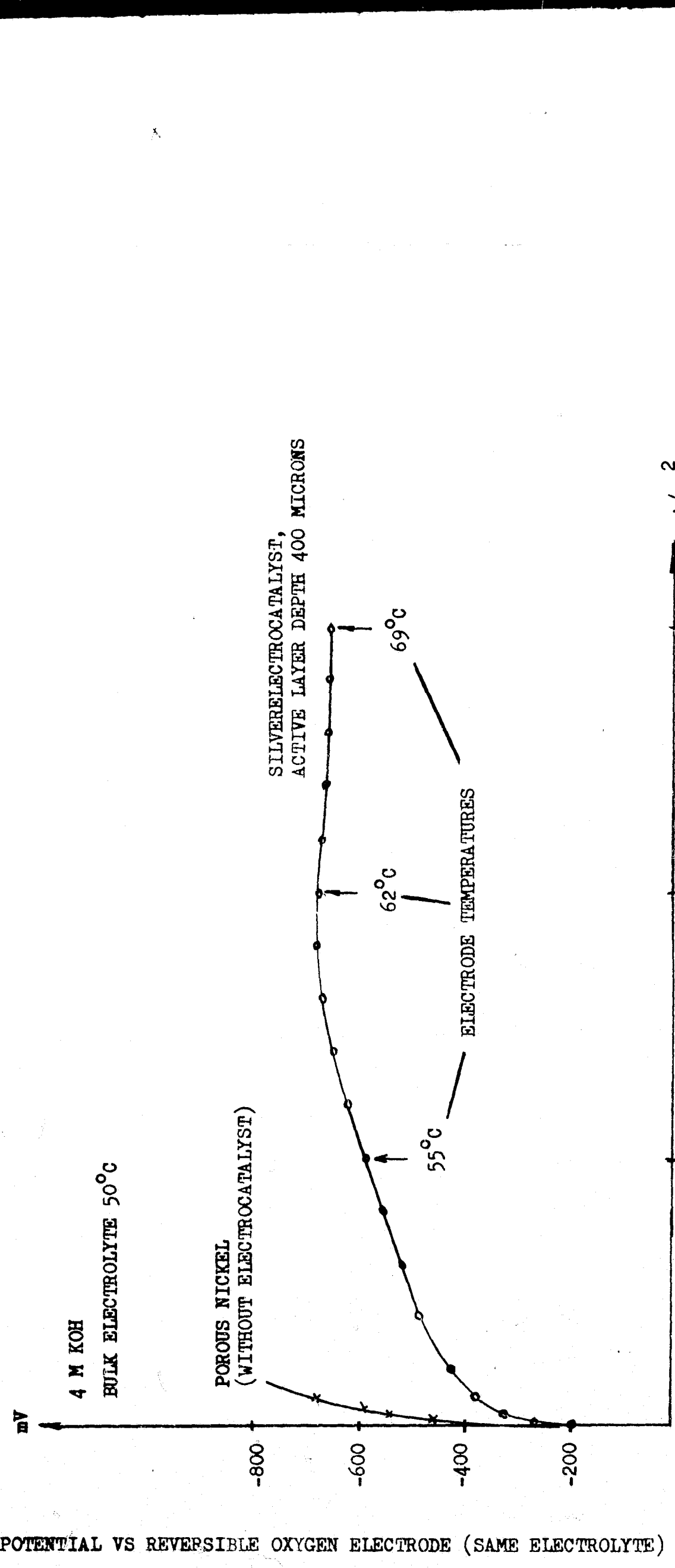

FIG. 11 POLARIZATION CURVES AT OPTIMUM DIFFERENTIAL PRESSURE 1.4 ATM WITH VARYING ELECTROLYTE CONCENTRATION SILVER ELECTROCATALYST, ACTIVE LAYER DEPTH 100 MICRONS

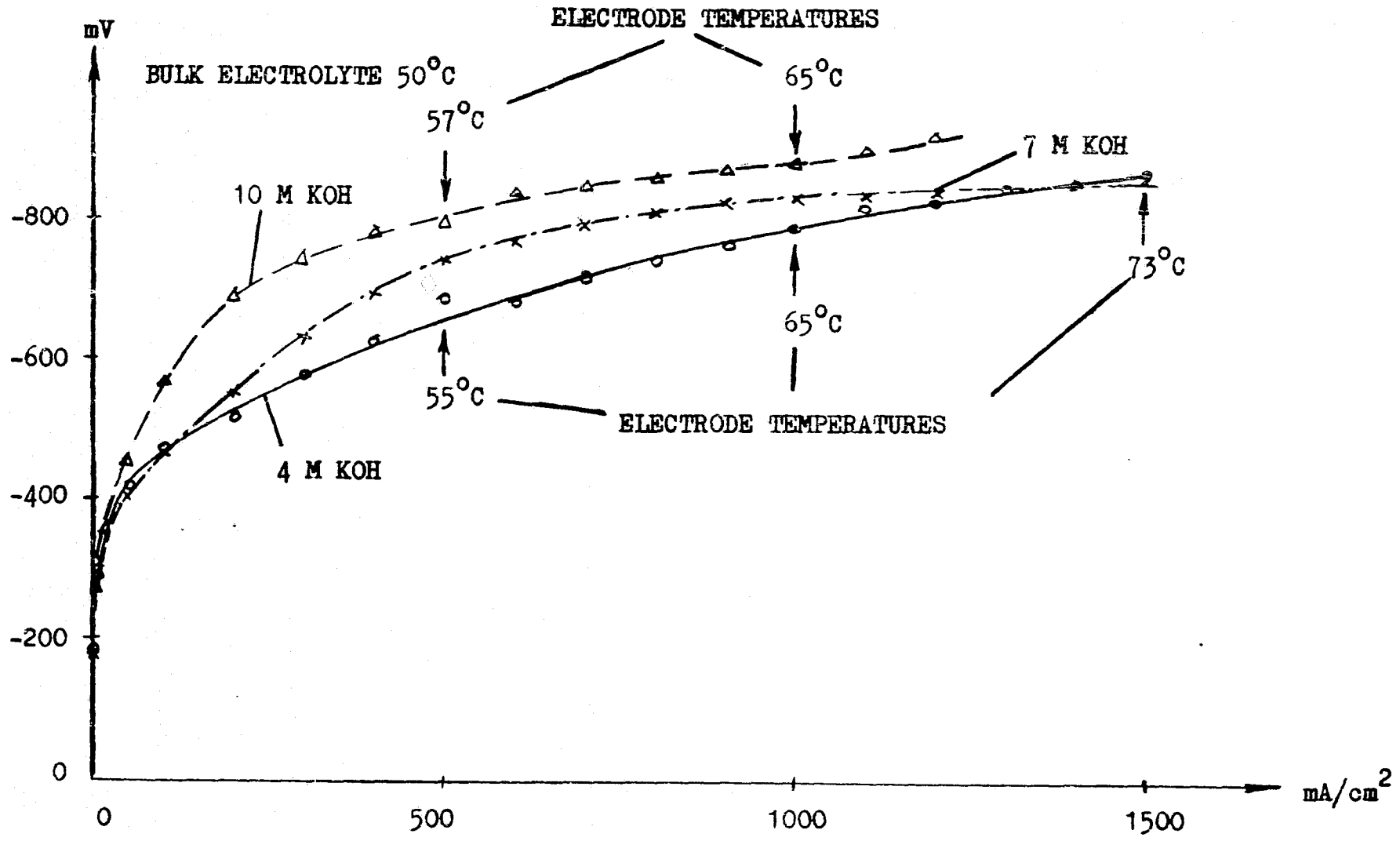

9
CALCULATIONS

9.1 Theoretical Model

In this thin film model, it is assumed that a thin film with constant thickness exists above the meniscus and is in contact with the solid phase in the pore. The following steps are incorporated.

(i) Diffusion of reactant gas, O_2 in inert gases, from outer end of the pore with a gas pressure P_o to gas/electrolyte interface

(ii) Radial diffusion of O_2 from gas/electrolyte interface $r = r_1$ through a thin liquid film to $r = r_2$ for $0 \leq Z \leq L$

(iii) Electrosorption and charge transfer of adsorbed oxygen.

(iv) Mass transport of ions along the liquid film.

Srinivasan and Hurwitz (13) have treated mathematically the "Thin-Film Model" for a combination of mass transport polarization. This treatment extends their solution to include mass transport in gaseous phase of mixed gases.

9.2 Solution of equations

Axial flow in through diffusion

$$\overset{o}{N}_{O_2}\Big|_z = -D_g \frac{dC(z,o)}{dz} \cdot \pi \cdot r_1^2 \qquad (1)$$

Axial flow out through diffusion

$$\overset{o}{N}_{O_2}\Big|_{z+dz} = -D_g \cdot \left(\frac{dC(z,o)}{dz} + \frac{d^2C(z,o)}{dz^2} \cdot dz\right) \cdot \pi \cdot r_1^2 \qquad (2)$$

Radial flow out through diffusion

$$\overset{o}{N}_{O_2}\Big|_{z,R} = -D_v \cdot \frac{dC(z,r)}{dr} \cdot 2 \cdot \pi \cdot r \qquad (3)$$

Reaction rate

$$\overset{o}{N}_{O_2}\Big|_{z,r} = \frac{dI}{n \cdot F} \qquad (4)$$

Mass balance. Axial flow in -Axial flow out

$$-D_g \cdot \frac{dC(z,o)}{dz} \cdot \pi \cdot r_1^2 - \left[-D_g \cdot \left(\frac{dC(z,o)}{dz} + \frac{d^2C(z,o)}{dz^2}\right) \cdot dz \cdot \pi \cdot r_1^2\right]$$

- Radial flow out = 0;

$$-\frac{dI}{n \cdot F} = 0 \qquad (5)$$

Polarization

$$dI = 2 \cdot \pi \cdot r_2 \cdot dz \cdot io \left\{\frac{C(z,r_2)}{C(z,o)} e^{\frac{\eta F}{2RT}} - e^{-\frac{\eta F}{2RT}}\right\} \qquad (6)$$

$$d\eta = I \frac{dz}{\mathcal{K} \cdot \pi \cdot (r_2^2 - r_1^2)} \qquad (7)$$

Concentration of oxygen

$$C(o,r_1) = P_o \cdot Sb_{O_2} \cdot X_{O_2} \qquad (8)$$

$$\text{Number of pores/cm}^2 = \frac{A_f}{2 \cdot \pi \cdot r_1 \cdot L} \qquad (9)$$

Current density

$$i = \frac{I \cdot A_f}{2 \cdot \pi \cdot r_1 \cdot L} \qquad (10)$$

Combining 3 and 4 we get

$$\frac{dI}{n \cdot F} = -2 \cdot \pi \cdot D_v \cdot dz \cdot \frac{dc}{\frac{dr}{r}}$$

integration with B.C. $C(z,r) = C(z,r_2)$ $C(z,r) = C(z,o)$

$r = r_2$ $r = r_1$

$$\int_{r_1}^{r_2} \ln r \cdot \frac{dI}{dz} = -n \cdot F \cdot 2 \cdot \pi \cdot D_v \int_{C(z,o)}^{C(z,r_2)} C$$

Rearranging gives

$$C(z,o) = C(z,r_2) + \frac{\frac{dz}{dz} \cdot \ln r_2/r_1}{2 \cdot \pi \cdot n \cdot F \cdot D_v} \qquad (3a)$$

Eqv. 5 gives $\quad D_g \frac{d^2C(z,o)}{dz^2} \cdot dz \cdot \pi \cdot r_1^2 = \frac{dI}{n \cdot F} \qquad (5a)$

Eqv. 6 gives $\quad C(z,r_2) = C(z,o) \quad \frac{\frac{dI}{dz \cdot 2 \cdot \pi \cdot r_2 \cdot i_o} + e^{-\frac{\eta F}{2RT}}}{e^{\frac{\eta F}{2RT}}}$

(6a)

Combining 3a and 6a gives

$$\frac{dI}{dz} = \frac{C(z,o)\ (1 - e^{-\frac{\eta F}{RT}}) \cdot 2 \cdot \pi \cdot n \cdot F \cdot D_v}{\ln r_2/r + \frac{n \cdot F \cdot D_v \cdot C(z,o) \cdot e^{-\frac{\eta F}{2RT}}}{r_2 \cdot i_o}}$$

If $\ln r_2/r_1 \gg \frac{n \cdot F \cdot D_v \cdot C(z,o) \cdot e^{-\frac{\eta F}{2RT}}}{r_2\ i_o}$ we get

$$\frac{dI}{dz} = \frac{C(z,o)\ (1 - e^{-\frac{\eta F}{RT}}) \cdot 2\pi \cdot n \cdot F \cdot D_v}{\ln r_2/r_1} \qquad (3b)$$

If $\ln r_2/r_1 \ll \frac{n \cdot F \cdot D_v \cdot C(z,o) \cdot e^{-\frac{\eta F}{2RT}}}{r_2 \cdot i_o}$ we get

$$\frac{dI}{dz} = (1 - e^{-\frac{\eta F}{RT}}) \cdot 2 \cdot \pi \cdot r_2 \cdot i_o \cdot e^{\frac{\eta F}{2RT}} \qquad (3c)$$

Using 3b together with 5a gives

$$\frac{d^2C(z,o)}{dz^2} - \frac{C(z,o)}{K} = 0 \qquad K = \frac{2 \cdot D_v \cdot (1 - e^{-\frac{\eta F}{RT}})}{r_1^2 \cdot D_g \cdot \ln r_2/r_1}$$

Laplace transformation gives

$$s^2 \cdot C(s,o) - s \cdot C(o,o) - \frac{dc(o,o)}{dz} - \frac{C(s,o)}{K} = 0$$

$$C(s,o) = \frac{dc(o,o)}{dz} \frac{1}{s^2 - \frac{1}{K}} + C(o,o) \cdot \frac{s}{s^2 - \frac{1}{K}}$$

$$C(z,o) = \frac{dc}{dz}(o,o) \cdot \sqrt{K} \cdot \sinh z \cdot \sqrt{\frac{1}{K}} + C(o,o) \cdot \cosh z \cdot \sqrt{\frac{1}{K}}$$

B.C. $\begin{cases} \frac{dC(z,o)}{dz} = 0 & C(z,o) = P_o \cdot X_{O_2} \cdot Sb_{O_2} \\ z = L & z = 0 \end{cases}$ gives

$$C(z,o) = P_o \cdot X_{O_2} \cdot Sb_{O_2} \cdot \cosh z \cdot \sqrt{\frac{2 \cdot D_v(1-e^{-\frac{\eta F}{RT}})}{r_1^2 \cdot D_g \cdot \ln r_2/r_1}} -$$

$$- Po \cdot X_{O_2} \cdot Sb_{O_2} \cdot \tanh L \cdot \sqrt{2\, D_v \cdot \frac{(1-e^{-\frac{\eta F}{RT}})}{r_1^2 \cdot D_g \cdot \ln r_2/r_1}} \cdot$$

$$\cdot \sinh z \cdot \sqrt{\frac{2\, D_v(1-e^{-\frac{\eta F}{RT}})}{r_1^2 \cdot D_g \cdot \ln r_2/r_1}} \qquad (5b)$$

Using 5b in 3b we get

$$dI = \frac{dz \cdot (1-e^{-\frac{\eta F}{RT}}) \cdot C(z,o) \cdot 2 \cdot \pi \cdot n \cdot F \cdot D_v}{\ln r_2/r_1} \qquad (11)$$

Solving 3c we get after Laplace transformation

$$s^2 \cdot C(s,o) - s^1 \cdot C(o,o) - \frac{dC}{dz}(o,o) - \frac{K^1}{s} = 0$$

$$K^1 = \frac{2 \cdot r_2 \cdot i_o \cdot (1-e^{-\frac{\eta F}{RT}})}{r_1^2 \cdot D_g \cdot e^{-\frac{\eta F}{2RT}}}$$

$$C(s,o) = C(o,o) \cdot \frac{1}{s} + \frac{dC(o,o)}{dz} \frac{1}{s^2} + \frac{K^1}{s^3} = 0$$

$$C(z,o) = C(o,o) + z \cdot \frac{dC(o,o)}{dz} + \frac{K^1}{2} \cdot z^2$$

With boundary condition

$$\frac{dC(z,o)}{dz} = 0 \qquad C(z,o) = P_o \cdot X_{O_2} \cdot Sb_{O_2}$$

$$z = L \qquad Z = 0$$

$$C(z,o) = P_o \cdot X_{O_2} \cdot Sb_{O_2} - \frac{z \cdot 2 \cdot r_2 \cdot i_o(1-e^{-\frac{\eta F}{RT}})}{r_1^2 \cdot D_g \cdot e^{-\frac{\eta F}{2RT}}} (L - \frac{z}{2}) \quad (5c$$

Using 5b in 3c gives

$$dI = dz \cdot (1-e^{-\frac{\eta F}{RT}}) \cdot 2\pi \cdot r_2 \cdot i_o \cdot e^{-\frac{\eta F}{RT}} \qquad (12)$$

11 and 12 can be solved numerical by a computer.
Eqv. 7 is introduced as a loop in the program.

L is divided into sections. By adding the current in the sections we can calculate i as a function of .

Calculation of diffusivity of oxygen in argon and in helium.

$$D_{O_2-x} = \frac{0.001858\sqrt{T^3\left(\frac{1}{M_{O_2}} + \frac{1}{Mx}\right)}}{P_o \cdot \delta_{O_2 x}^2 \cdot \Omega_{0.02x}} \qquad \text{(Chapman-Enskog)}$$

ARGON

M_{O_2} = 32.000 δ_{O_2} = 3.433 Å $\frac{\varepsilon}{K}$ = 113°K

M_{Ar} = 39.944 δ_{Ar} = 3.418 Å $\frac{\varepsilon}{K}$ = 124°K

M_{He} = 4.003 δ_{He} = 2.576 Å $\frac{\varepsilon}{K}$ = 10.2°K

$\delta_{O_2\text{-}Ar} = \frac{1}{2}(3.418 + 3.433) = 3.426$ Å

$$\frac{\varepsilon_{O_2\text{-}Ar}}{K} = \sqrt{124 \cdot 113} = 118.5^\circ K \qquad \frac{KT}{\varepsilon_{O_2\text{-}Ar}} = \frac{323}{118.5} = 2.727$$

in tables we get $D_{ArO_2} = 0.974$

$$D_{O_2\text{-}Ar} = \frac{0.001858\sqrt{323.15^3\left(\frac{1}{32} + \frac{1}{39.944}\right)}}{1 \cdot 3.426^2 \cdot 0.974} = 0.224 \ \frac{cm^2 \cdot atm}{s}$$

P_o = 1.8 atm $\qquad D_{O_2}$ - Ar = 0.124 cm^2/s

HELIUM

$$D_{He-O_2} = \frac{0.001858\sqrt{323.15^3\left(\frac{1}{32}+\frac{1}{4.003}\right)}}{1 \cdot 3.004^2 \cdot 0.6231} = 1.0168 \ \frac{cm^2 \cdot atm}{s}$$

$P_o = 1.8$ atm $\quad \underline{D_{He-O_2} = 0.565 \ cm^2/s}$

Nomenclature

T	Electrode temperature	^{o}K
R1	Inner pore radius	cm
R2	Outer pore radius	cm
R2-R1	Filmthickness	cm
L	Pore depth	cm
P_o	Total pressure	atm
Sb_{O_2}	Solubility of oxygen	$mol/cm^2 \cdot atm$
D_{O_2}-Ar	Diffusivity of oxygen in argon	cm^2/s
D_{O_2}-He	Diffusivity of oxygen in helium	cm^2/s
X_{O_2}	Mole fraction of oxygen	
A_f	Film surface at 1.8 atm	cm^2/cm^2 geom. area
D_v	Diffusivity of oxygen in 4 M KOH	$cm^2/sec.$
R	Gas constant	I/mole.deg.
C(z,r)	Concentration of O_2 at z,r	$mole/cm^3$
$\mathcal{H}$	Ionic conductivity in 4 M KOH	$ohm^{-1}cm^{-1}$
$N_{O_2}/_{z,r}$	Molar flow of O_2 at z,r	$mol/cm^3 \cdot$ sec.
i_o	Exchange current	A/cm^2
I	Current	A/pore
i	Current density	A/cm^2 geom. area
η	Polarization	Volt
n·F	Faradays number	As

9.3
ALGOL-program

It is not possible to obtain analytical solutions for current density/overpotential and current distribution. Numerical calculation were therefore carried out with a computer.

The calculation involved current distribution, current density and concentration profiles. By setting D_g to 10^2 or higher the equation correspond to Srinivasan and Hurwitz solution for thin film model.

The input parameters are R_1, R_2, L, A_f, D_v, D_g, $Sb0_2$, X_{O_2}, P_o, i_o, T, α, n all as a function of varying polarization.